Ferromagnetism and stability of half-metallic MnSb and MnBi in the strained zinc-blende structure: Predictions from full potential and pseudopotential calculations

Jin-Cheng Zheng and James W. Davenport
Center for Data Intensive Computing, Brookhaven National Laboratory, Upton, New York 11973, USA
(Received 7 September 2003; revised manuscript received 22 December 2003; published 14 April 2004)

We use first principles calculations to study the energy and magnetic moment of MnSb and MnBi in the (equilibrium) nickel arsenide, zinc-blende, and tetragonally distorted zinc-blende structures. We find that the zinc-blende structure is mechanically unstable, i.e., the energy is a relative maximum for $c/a=1$ at fixed volume. We studied the tetragonal structures by fixing the in-plane lattice constant to be equal to that of typical semiconductors (such as GaAs) which might serve as substrates for epitaxial growth and then minimizing the energy as a function of c/a. Over a wide range of a, including that of GaAs, we find half-metallic ferromagnets. We suggest that these structures are much more likely to be achieved as thin films than the cubic zinc-blende phases.

DOI: 10.1103/PhysRevB.69.144415 PACS number(s): 75.90.+w, 71.20.−b, 75.50.−y, 75.30.−m

I. INTRODUCTION

Recently, there has been an increased interest in diluted magnetic semiconductors, which are promising materials for innovative spin-based devices.[1] The field of spintronics has attracted considerable attention because it offers unique opportunities for a new generation of multifunctional devices utilizing conventional charge-based microelectronics with the addition of the spin degree of freedom.[2] Such coupling of electron charge and spin has led to such interesting applications as ''spin field effect transistors,'' [3] ''spin valves,'' [4] and ''spin qubits.'' [5]

These diluted magnetic semiconductors are mainly based on III-V and II-VI semiconductors doped with manganese. Recent theoretical calculations[6] predicted that MnSb and MnBi would show half-metallic ferromagnetism in the zinc-blende (ZB) structure. In half-metallic systems, there is only one electronic spin direction at the Fermi energy; therefore such systems have unique properties and are the ideal components for spintronic devices. Many half-metallic ferromagnets have been recently found in experiments (e.g., NiMnSb,[7] CrO_2,[8] Fe_3O_4,[9] and the colossal magnetoresistance manganite materials[10]) or predicted from theoretical calculations.[11–20]

In theoretical calculations of Mn pnictides, the effect of uniform volume changes on magnetic properties has been considered. However, very little attention has been paid to the effect of nonuniform strains on the stability and magnetic properties. Since the bulk ZB structure of Mn compounds is unstable, the epitaxial growth of Mn pnictide thin films or multilayers on III-V or II-VI semiconductors, or formation of nanostructures such as nanodots embedded in semiconductor thin films, or superlattices with semiconductors, is expected to be achieved. In such cases, strains inside the films, multilayers, nanostructures, and superlattices are expected to play an important role in the stability and electronic and magnetic properties. To investigate this issue, we have performed full potential and pseudopotential first principles calculations based on density functional theory[21] (DFT) for MnSb and MnBi.

The outline of the paper is as follows. In Sec. II, the computational details of the full potential and pseudopotential methods are described. After we obtain the structural and magnetic properties of MnSb and MnBi in the NiAs and ZB structures in Sec. III, we then present in Sec. IV the results for the strained ZB structure for both compounds, including an examination of the stability of the ZB structure due to strains, properties of the tetragonal structure, and enhancement of the range of half-metallic ferromagnetism in ideal thin films. The spin-orbit coupling effects are discussed in Sec. V. Finally, we conclude our results in Sec. VI.

II. COMPUTATIONAL METHODS

All calculations in this work were performed by first principles methods based on density functional theory.[21] We have used both full potential and pseudopotential methods to calculate the structural, electronic, and magnetic properties of Mn pnictides (i.e., MnSb and MnBi) in several structural forms such as NiAs-type (NA), ZB, and tetragonal (TET) phases. The technical details are described in the following.

A. Full potential method

The full potential calculations were performed using WIEN2K,[22] a full potential (linear) augmented plane wave plus local orbitals method within DFT.[21] The generalized gradient approximant (GGA) proposed by Perdew, Burke, and Ernzerhof[23] was used for exchange and correlation. Most calculations were performed using the scalar relativistic approximation for the valence states, but spin-orbit coupling was added as a check in selected cases (see Tables I and III below). It was found that inclusion of spin-orbit coupling did not change the ordering of the structures but did affect the band gap, as described in Sec V. Muffin-tin radii (R_{MT}) of 2.40 bohr were chosen for Mn, Sb, and Bi, and $R_{MT}K_{max}$ was taken to be 8.0. An angular momentum expansion up to $l_{max}=10$ for the potential and charge density representations was used in the calculations. At convergence the integrated difference between input and output charge densities was less than 10^{-4}. For all structures, 3000 k points were used

TABLE I. All-electron vs pseudopotential calculations for MnSb and MnBi in NiAs (NA) structure (space group $P6_3/mmc$, no. 194) [AE: all-electron (WIEN2K); PS: pseudopotential (SIESTA)]. Values in parentheses are the magnetic moments including spin-orbit coupling.

Method	MnX	a_{MnX} (Å)	c_{MnX} (Å)	c/a	V_0 (Å^3/unit)	μ_{MnX} (μ_B)	Reference
AE	MnSb	4.120	5.673	1.377	41.70	3.25(3.27)	This work
PS		4.190	5.732	1.368	43.54	3.48	This work
Other calc		4.128	5.573	1.35	41.12	3.25	12
Expt.		4.15	5.78	1.39		3.57	32
AE	MnBi	4.283	5.868	1.370	46.60	3.54(3.58)	This work
PS		4.373	5.991	1.370	49.49	3.77	This work
Expt.		4.341	5.973	1.376	48.74	3.8	32(a)
Expt.		4.2827	6.1103			3.60	32(b)

for the Brillouin-zone integrations. Convergence was checked by increasing the number of k points. The numerical error was less than 1 meV/atom for energy and $0.001\mu_B$ per Mn atom for magnetic moment.

B. Pseudopotential method

For the pseudopotential calculations, we used the SIESTA code,[24] which is a fully self-consistent DFT method based on a linear combination of atomic orbitals (LCAO) basis set with linear scaling. Details can be found in a recent review.[25] The double-ζ plus polarization (DZP) basis set (15 orbitals for Mn and 13 orbitals for both Sb and Bi, with cutoff radius of about 8 a.u.), which has been shown to yield high-quality results for most of the systems studied, was used in this work. Norm-conserving pseudopotentials for Mn, Sb, and Bi were generated using the Troullier-Martins scheme[26] within the generalized gradient approximation[8] including scalar relativistic effects. We then transformed the semilocal form into the fully nonlocal form proposed by Kleinman and Bylander (KB).[27] The reference electron configuration for Mn was $4s^{1.75}\ 4p^{0.25}\ 3d^5$ with core radii of 2.0, 2.20, and 1.80 a.u., for Sb $5s^2\ 5p^3\ 5d^0$ with core radii of 2.60, 2.60, and 2.60 a.u., and for Bi $6s^2\ 6p^3\ 6d^0$ with core radii of 2.20, 2.90, and 2.90 a.u., respectively. A partial-core correction for the nonlinear exchange correlation[28] with pseudocore radius of 0.70 a.u. for the nonlinear exchange correlation was included for Mn to obtain reliable moments on the magnetic atoms. For Sb and Bi, the pseudocore radii were 1.77 a.u. and 1.95 a.u., respectively. We have compared the one-electron eigenvalues and the excitation energies for all elements in various electron configurations obtained from the pseudopotentials with those from all-electron atomic calculations. The maximum error in the magnitude was found to be less than 1%. The special k points (about 140–200 k points in the irreducible Brillouin zone) used in this work were generated by the Monkhorst-Pack scheme.[29] It was found that such k point sampling led to numerical errors less than 1 meV/atom in total energy and $0.001\mu_B$ per Mn atom in magnetic moment.

III. STRUCTURAL AND MAGNETIC PROPERTIES OF MnSb AND MnBi IN NiAs AND ZB STRUCTURES

A. Ground-state NiAs phase of MnSb and MnBi

First, we examined the structural, electronic, and magnetic properties of MnSb and MnBi in the NA ground-state structure and compared the results with experimental data and other calculations. The NA structure is hexagonal, space group $P6_3/mmc$ (no. 194). The calculated lattice parameters are listed in Table I. Our lattice constants from both the full potential and the pseudopotential methods are generally in good agreement with experimental data and previous calculations. The predicted ferromagnetic moments are also close to the experimental values with differences less than $0.3\mu_B$. Most of this difference is due to the different lattice constants. At the same lattice constant as that of the full potential calculation the difference is only $0.11\mu_B$. The agreement with experimental results for the NA structure demonstrates the validity of the current calculations. Therefore, we proceeded to calculate the high-energy structure (ZB phase) and its strained structure.

TABLE II. All-electron vs pseudopotential calculations for MnSb and MnBi in ZB structure (space group $F\bar{4}3m$, no. 216) [AE: all-electron (WIEN2K); PS: pseudopotential (SIESTA)].

Methods	MnX	a_{MnX} (Å)	V_0 (Å^3/unit)	B (GPa)	μ_{MnX} (μ_B)	Reference
AE	MnSb	6.203	59.66	44	4.00	This work
PS		6.254	61.16	44	4.00	This work
Other calc		6.166			3.77	12
Other calc					4.00	6
AE	MnBi	6.400	65.54	39	4.00	This work
PS		6.431	66.49	37	4.00	This work
Other calc		6.399			4.00	6

B. ZB structure of MnSb and MnBi

For the ZB structure (space group $F\bar{4}3m$, no. 216), our calculated lattice constants are 6.203 Å and 6.254 Å for MnSb, 6.400 Å and 6.431 Å for MnBi, by full potential and pseudopotential calculations, respectively. The calculated lattice parameters are in good agreement with previous calculations, as shown in Table II. We note that the lattice constants calculated from the pseudopotential method for both MnSb and MnBi in both NA and ZB structures are slightly larger than those from the full potential method. However the agreement is still quite good because the discrepancies are less than 1%.

The calculated ferromagnetic moments for both compounds at the equilibrium volume are $4.00\mu_B$ by both full potential and pseudopotential calculations. Our calculations show that both MnSb and MnBi are half-metallic ferromagnets within the GGA, in good agreement with calculations by Xu *et al.*[6] but in disagreement with Ref. 12. As pointed out by Xu *et al.*,[6] this may be due to insufficient k point sampling or a too low energy cutoff in the plane-wave expansion used in the previous calculation.[12]

The spin-polarized band structures of MnSb and MnBi in the ZB structure obtained by pseudopotential calculations are illustrated in Fig. 1. It is clear that the band structure is metallic for the majority spin electrons (spin up) and semiconducting for the minority spin electrons (spin down). The band structures calculated from the full potential method are in good agreement with those from the pseudopotential method with only a slight difference in the band gap of the minority spin electrons.

We obtained the magnetic moments of ZB MnSb and MnBi as a function of volume and found that ZB phases maintain full half-metallic ferromagnetism up to 5% and 15% compression for MnSb and MnBi, respectively. We note that in nonrelativistic calculations the range of compressed volume will be smaller. In the range of large volume (greater than the equilibrium volume), both MnSb and MnBi remain half-metallic ferromagnets. Our calculations confirm from both full potential and pseudopotential methods that MnBi is a robust full half-metallic ferromagnet against volume changes, which is in agreement with the prediction by Xu *et al.*[6] Very nice discussions of the origin of the half-metallic ferromagnetism in Mn compounds have been given by de Groot *et al.*[30] and by Xu *et al.*[6]

IV. STRUCTURAL AND MAGNETIC PROPERTIES OF MnSb AND MnBi IN STRAINED ZB STRUCTURES

In the previous section, we showed that ZB MnSb and MnBi are full half-metallic ferromagets in the GGA. This interesting property of these compounds will promote further research on their applications in spintronics devices. In practice, some fundamental (also practical) issues regarding stability need to be addressed. For example, is the bulk ZB structure unstable or metastable? Is it possible to stabilize the ZB structure in thin films grown epitaxially on semiconductor substrates? To investigate these questions we performed calculations on strained MnSb and MnBi.

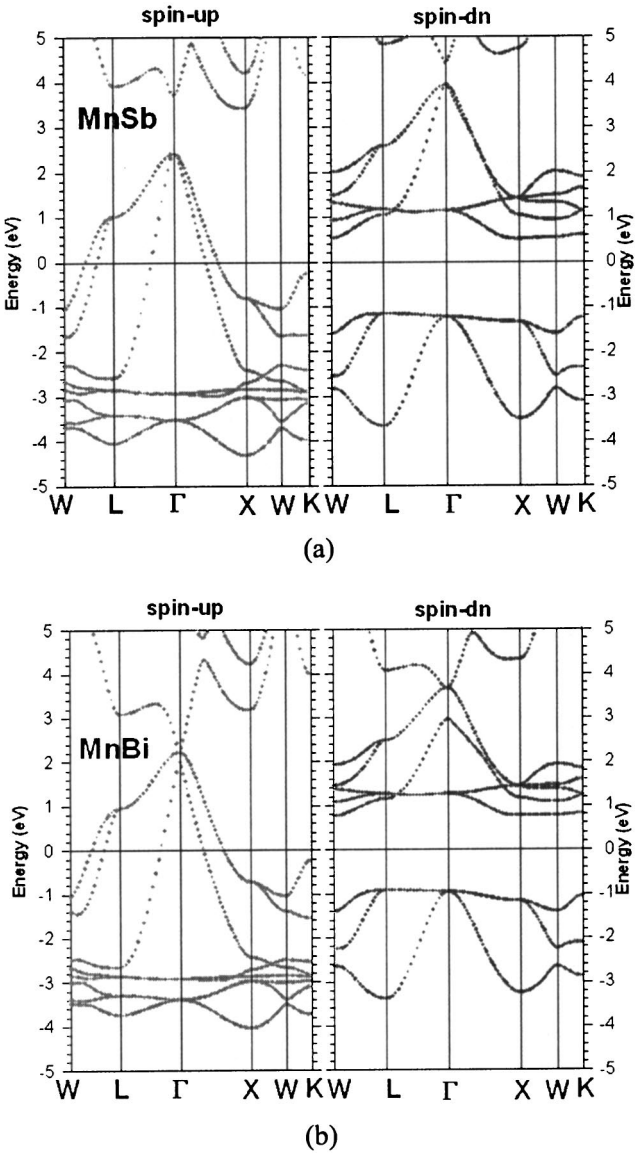

FIG. 1. Band structure of ZB MnSb (a) and MnBi (b). The deeper valence band from Sb 5s and Bi 6s is not shown in the figure.

A. Instability of the ZB structure of MnSb and MnBi

The stability of ZB MnSb and MnBi was examined by calculation of the total energy change with regard to tetragonal strains in the c direction of the crystal structure. The total energies as a function of c/a (keeping the volume equal to the equilibrium volume of the ZB phase) are illustrated in Fig. 2. We find that both compounds are mechanically unstable. That is, the energy is a relative maximum at $c/a=1$. The compounds will stabilize into two tetragonal phases with either $c/a>1$ or $c/a<1$, as shown in Fig. 2. The total energy as a function of c/a shows two local minima, one at $c/a \sim 1.25$ and the other with lower energy at 0.75. Interestingly, the ferromagnetic moments of both MnSb and MnBi in the range of c/a studied (as shown in Fig. 2) at equilibrium volume remain constant, at $4.000\mu_B$, i.e., half-metallic ferromagnetic. Given the shape of the energy versus c/a, it is

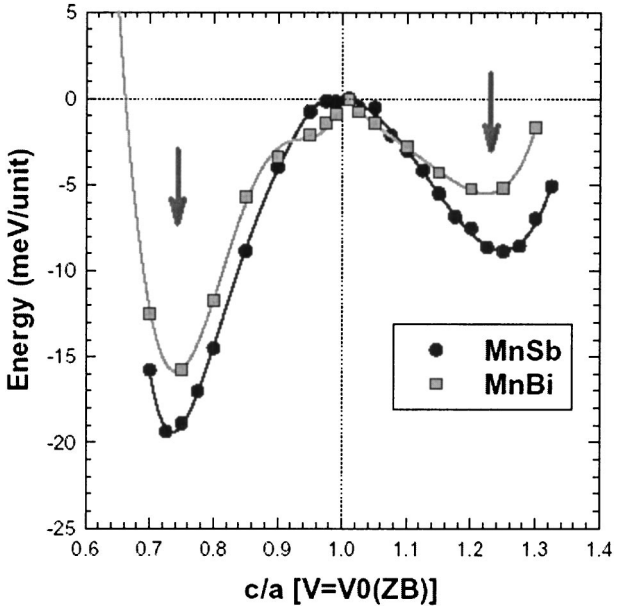

FIG. 2. The stability of MnSb and MnBi at equilibrium volume of the ZB structure as a function of c/a. The ferromagnetic moments for MnSb and MnBi remain $4.00\mu_B$ (i.e., half-metallic ferromagnetic) in the whole range of c/a considered.

clear that a normal mode analysis would yield negative phonon frequencies, although we did not perform such an analysis.

To examine the stability of the ZB structure, we present in Fig. 3 a comparison of the total energies for ZB, NA, and strained ZB (TET) structures.

The reason why MnSb and MnBi cannot be stabilized into the ZB structure can be understood in terms of an analysis of the electronic bonding configurations. Mn has the electronic configuration of $3d^5 4s^2$, and Sb (or Bi) has the typical group V electronic configuration s^2p^3. MnSb (or MnBi) has 12 electrons per formula unit, which is four electrons more than the eight required to form tetrahedral bonding as in a typical III-V or II-VI or- IV semiconductor. The strong electrostatic energy due to the excess electrons will lead to a distortion of the tetrahedral bonds. The origin of the instability of the ZB structure due to nonstoichiometric configurations has been discussed recently by Zheng *et al.*[31] A similar situation occurs in group IV-V compounds[31] such as carbon nitride or carbon phosphide with 1:1 stoichiometry, they have nine electrons per formula unit, thus leading to distortion of the ZB structure and are then stabilized into tetragonal, rhombohedral, or hexagonal structures.

Considering the instability of the ZB structure, our calculations indicate that it is not likely to form in the cubic ZB phase in bulk MnSb and MnBi. Even in thin films (epitaxial growth of the ZB phase on semiconductor substrates), the ZB phase is expected to be unstable since it is easier to undergo a phase transition from the ZB to the tetragonal phase due to anisotropic stress from the interface between films and substrates. It may be possible to form the ZB structure in dilute II-V, III-V, or III-IV ZB semiconductors by doping with Mn, because a small amount of Mn can be confined in the local tetrahedral environment by the parent nonmagnetic semiconductors. A more complicated case occurs for MnSb and MnBi nanostructures. The stability of the ZB phase in nanostructures will mainly depend on the competition between geometrical confinement by the surrounding matrix and the intrinsic stress inside the pnictides. Such competition limits the size of nanoparticles (quantum dots) in the ZB structure and also the solubility of Mn in semiconductors.

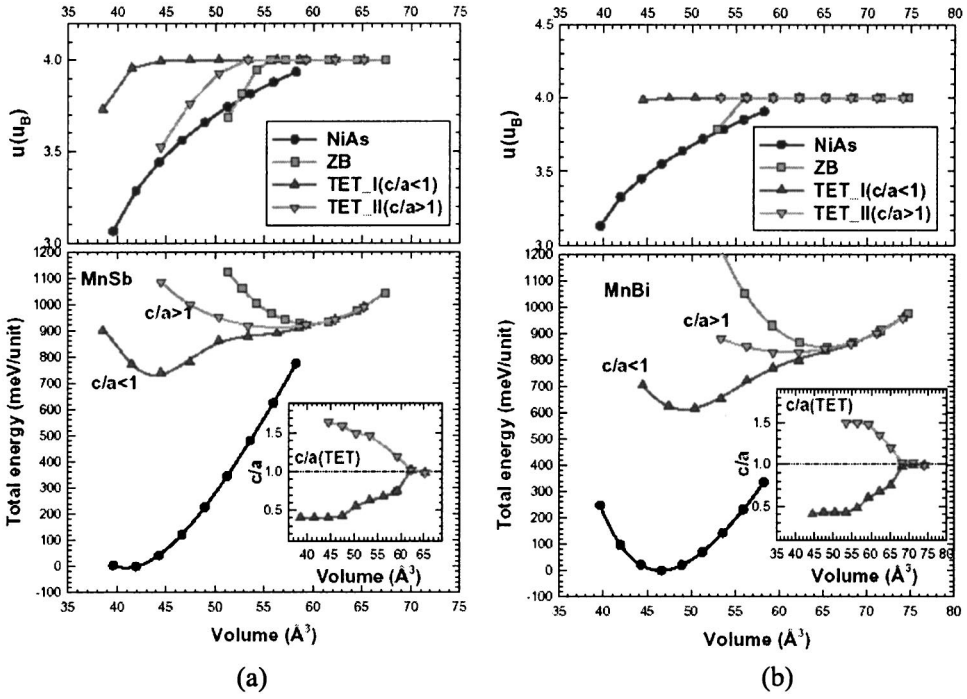

FIG. 3. Total energy and magnetic moment of different phases of MnSb and MnBi as a function of volume. The c/a of the tetragonal phases are shown in the inset.

TABLE III. Full potential calculations for MnSb and MnBi in tetragonal structure (space group $I\bar{4}m2$, no. 119). [TET(I) and TET(II) refer to tetragonal phase with $c/a<1$, and $c/a>1$, respectively. ΔE (meV/unit) is the energy gain of the tetragonal phase compared with the ZB phase.] Values in parentheses are the energies including spin-orbit coupling.

Structure	a_{MnX} (Å)	c_{MnX} (Å)	c/a	V_0 (Å^3/unit)	μ_{MnX} (μ_B)	ΔE (meV/unit)
			MnSb			
TET(I)	7.632	3.053	0.400	44.46	4.00	−187 (−181)
TET(II)	5.250	7.743	1.475	53.35	4.00	−10 (−5)
			MnBi			
TET(I)	7.798	3.314	0.425	50.38	4.00	−231 (−313)
TET(II)	5.437	8.020	1.475	59.27	4.00	−19 (−20)

B. Tetragonal structure of MnSb and MnBi

To find the optimized structure of tetragonal MnSb and MnBi, we varied the volume of the unit cell and optimized c/a at each volume. The total energies as a function of volume for MnSb and MnBi are shown in Fig. 3, together with those for the NA and ZB phases. The optimized c/a at each volume for the tetragonal phases is also shown in the inset. At large volume, the ZB phase is metastable (NA is still lower in energy). With decreasing volume, two dense TET phases become metastable, one with c/a less than 1 and one with c/a larger than 1, and both have smaller volume. The TET phase with $c/a<1$ [TET(I)] is more stable than that with $c/a>1$ [TET(II)], and its density is comparable with that of the hexagonal NA phase. The detailed structural information about the TET phases is shown in Table III. The optimized c/a of MnSb is 0.400 for TET(I) and 1.475 for TET(II). For MnBi, the optimized c/a is 0.425 for TET(I) and 1.475 for TET(II).

Comparing the total energy of the tetragonal phase with that of the ZB phase, we find that TET(I) gains about 0.2 eV/formula unit while TET(II) gains only about 10% of that for TET(I) for MnSb and MnBi. Both the TET(I) and TET(II) phases have total energies larger than the NiAs phase. Therefore, the TET phases are metastable. They could possibly be stabilized in a superlattice, thin film, or nanostructure grown on ZB semiconductor substrates.

We find that both compounds in the TET phases are half-metallic ferromagnets. The half-metallic ferromagnetism extends to smaller volumes than for the ZB phase. The magnetic moments of the tetragonal phases are $4\mu_B$ (half magnetic) in a large volume range, still keep the same value at small volume, and then drop to smaller values for smaller volumes. It is interesting to see from Fig. 3 that the magnetic moments of the tetragonal phases are always larger than those of the ZB and NA phases in the whole range of volume studied. Therefore, our calculations indicate a possible way to control the magnetic moment by applying a strain field in these materials.

C. Extended range for half-metallic magnetism in distorted structures

In practice these materials would likely be grown as thin films on substrates such as GaAs. In view of their tendency to form tetragonal structures we have studied the electronic and magnetic properties as a function of in-plane lattice constant (a) and for calculated equilibrium c/a ratios.

It has recently been suggested by Xu *et al.*[6] that MnBi could be grown epitaxially on CdTe or InSb. It has also been reported that ZB MnAs,[33] CrAs,[34,35] and CrSb (Ref. 36) can be grown as nanodots and thin films or multilayers on a GaAs substrate. However, there are as yet no reports of successful growth of ZB MnSb and MnBi on semiconductor substrates. As we clearly show in Fig. 2 and Fig. 3, the ZB phase of MnSb and MnBi will be more likely to undergo a cubic-tetragonal phase transition, especially in the case of growth of thin films or multilayers on semiconductor substrates, since a strain field will be created due to lattice mismatches between MnSb (or MnBi) and the substrate. Therefore, the obtained structure of the epitaxial film will likely be either the TET structure or the NA ground state, depending on growth conditions. It would be interesting to investigate the magnetic properties of MnSb (or MnBi) in thin films growing on semiconductors. There are many factors that can affect the structural and magnetic properties of MnSb (MnBi) on semiconductor substrates, such as the interfacial geometrical structure, bonding configuration, charge transfer, effect of strains, and so on. For simplicity, we will limit our discussion to the case where the lateral lattice constants are constrained by the semiconductor substrate, and the perpendicular lattice constants are relaxed to minimize the total energy. In this simple model, it is possible to compare the effect of strains on the magnetism of MnSb and MnBi. This comparison is shown in Fig. 4. The c/a for the tetragonal phase is also shown. It is interesting that the range over which the half-metallic magnetism is observed is enhanced due to the tetragonal strain: it is extended to smaller in-plane lattice constants. To clearly illustrate this point, we compare in Fig. 5 the band structures of MnBi in the uniformly compressed ZB structure with lattice constant equal to that of GaAs (i.e., $a=5.65$ Å), and in the strained structure ($a=5.65$ Å and $c/a=1.345$). From the figure it can be seen that the Fermi energy of the compressed ZB structure is shifted to higher energy so that it overlaps the conduction band of the spin-down electrons; thus its half-metallic characteristic has been lost. The moment is correspondingly reduced from $4.000\mu_B$ to $3.279\mu_B$. In contrast, for strained MnBi, the Fermi energy is still in the band gap of the spin-

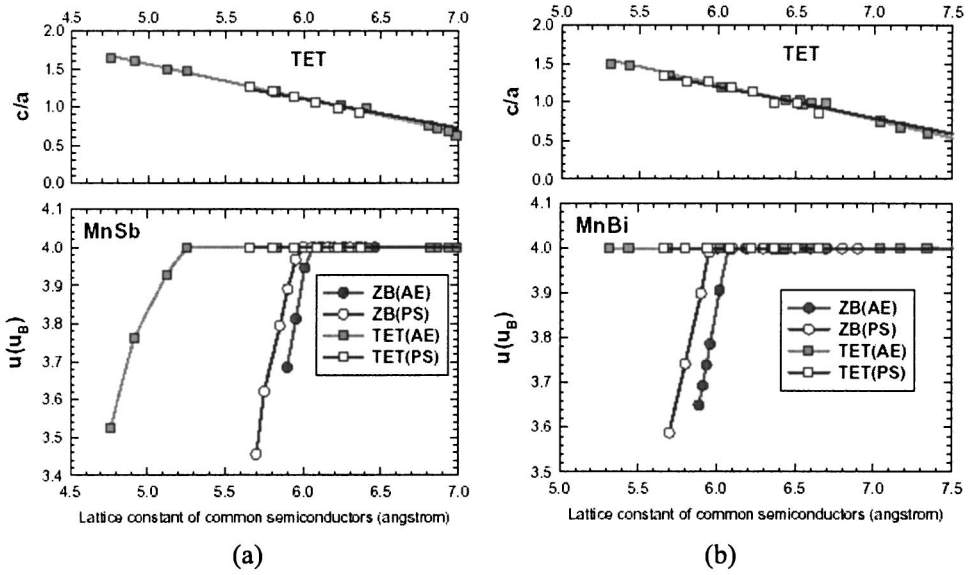

FIG. 4. Comparison of magnetic moments for MnSb and MnBi in ZB structure and tetragonal structure as a function of lattice constant of semiconductor substrates. Lattice constants (unit of Å) of common ZB semiconductors: InN (4.98), ZnS (5.41), Si (5.43), GaP (5.45), Ge (5.65), GaAs (5.65), ZnSe (5.67), CdS (5.82), InP (5.87), CdSe (6.05), InAs (6.06), GaSb (6.10), ZnTe (6.10), InSb (6.48), and CdTe (6.49) (Ref. 42). AE refers to all-electron calculations (WIEN2K), and PS is pseudopotential calculations (SIESTA).

down electrons with a ferromagnetic moment of $4.000\mu_B$. Therefore, the strained MnBi with in-plane lattice constant matching GaAs remains a half-metallic ferromagnet. This finding is encouraging, because our calculations show that the formation of thin films of MnSb or MnBi on common semiconductor substrates will not cause loss of the half-metallic magnetism, but will make it robust over quite a wide range of substrate lattice constant. However, we should state again here that the above conclusion is based on a simple strain model without consideration of interface bonding effects between MnSb (or MnBi) and the substrate. Such interfacial effects could play a significant role in the electronic and magnetic properties of MnSb (or MnBi). Detailed investigation of this issue is in progress.

The mechanism of the enhanced ferromagnetism in strained MnSb (or MnBi) lies in two factors: (i) the different crystallographic phases, and (ii) the relationship between bond length and magnetism of Mn atoms in Mn pnictides (see Fig. 6). It can be seen from Fig. 3 that for Mn pnictides, in the ZB or TET structure, the magnetic moment of Mn decreases with decreasing volume (accordingly, decreasing lattice constant or bond length of Mn-Mn). In uniformly compressed ZB MnSb (or MnBi), the Mn-Mn bond length decreases with decreasing lattice constant. However, in the strained MnSb and MnBi case, when the in-plane lattice constant (which is constrained by the substrate) decreases (is less than the equilibrium ZB lattice constant) c/a increases, as shown in Fig. 4, and the bond length for lateral (in-plane) Mn-Mn decreases but the bond length for perpendicular Mn-Mn increases accordingly. Thus the average bond length of Mn-Mn in strained MnSb (or MnBi) is larger than in the uniform compressed ZB structure, and therefore the ferromagnetism is enhanced in strained MnSb (or MnBi). For example, if the in-plane lattice constant is reduced from 6.10 Å (experimental lattice constant of GaSb) to 5.65 Å (experimental lattice constant of GaAs), the bond length of Mn-Mn is changed from 4.31 Å to 4.00 Å in uniform compressed ZB MnSb. For strained MnSb, the lateral bond length of Mn-Mn is the same as that of ZB MnSb, i.e., it changes from 4.31 Å to 4.00 Å, but the perpendicular Mn-Mn bond length increases from 4.47 Å to 4.57 Å. The same phenomenon is observed in MnBi.

V. SPIN-ORBIT COUPLING

Several authors have noted that the spin-orbit interaction does not qualitatively change the results for MnBi.[6,12] This may seem surprising since the spin-orbit splitting of the bismuth $6p$ level is 1.85 eV, comparable to the direct gap (at Γ) in the minority spin band, which is 2.1 eV. In contrast the spin-orbit splitting of the manganese $3d$ level is only 0.1 eV, while that for antimony $5p$ is 0.64 eV.

We can understand this in the following way. In a typical zinc-blende semiconductor, such as GaAs, the valence band maximum at Γ is sixfold degenerate (counting spin) in the absence of spin-orbit coupling and splits into twofold (Γ_7) and fourfold (Γ_8) states when spin-orbit coupling is included.[37] This picture is modified in MnBi as a result of the spin polarization so that the remaining degeneracy is removed.

As a simple model, consider a p state with combined hybridization and magnetic exchange splitting Δ and spin-orbit splitting parameter ζ. For $\Delta=0$ we obtain the usual spin-orbit doublet with energies $\zeta/2$ and $-\zeta$ for $p_{3/2}$ and $p_{1/2}$, respectively. For $\zeta=0$, we obtain threefold degenerate states at 0 and Δ. In our case, $\Delta\sim 3$ eV and $\zeta\sim 1.2$ eV (2/3 the atomic splitting). For $\Delta>\zeta$ the states lie approximately at Δ, $\Delta+\zeta/2$, $\Delta-\zeta/2$ and 0, $\zeta/2$, $-\zeta/2$. Hence the splitting of the lower band (spin down, valence band maximum) is approximately $\zeta\sim 1.2$ eV. The direct gap at Γ is reduced by $\sim\zeta/2$, or ~ 0.6 eV. We note that this is significantly less than might have been expected from the splitting of the atomic p level (i.e., $\Delta=0$). We have assumed that the conduction band minimum, composed predominantly of manganese d states, is hardly changed.

In order to test these ideas we calculated the band structure including spin-orbit coupling using WIEN2K.[22] In this code the spin-orbit coupling parameter for the valence states

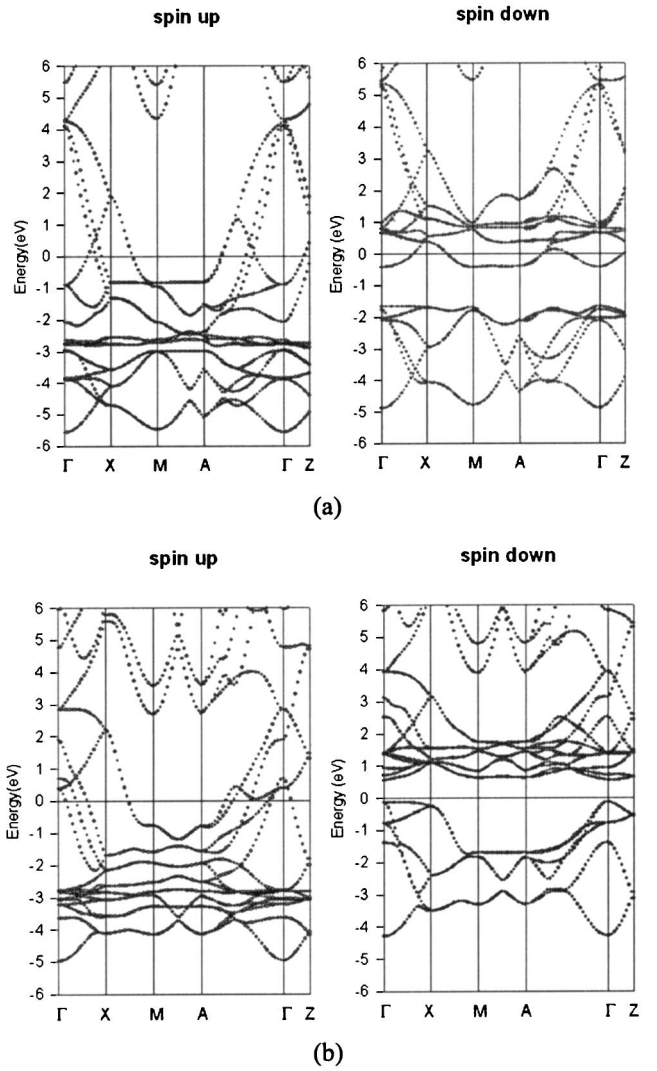

FIG. 5. Band structure of MnBi along symmetry lines of tetragonal Brillouin zone. (a) Uniformly compressed ZB MnBi with lattice constant equal to GaAs ($a=b=c=5.65$ Å); the magnetic moment is $3.279\mu_B$ (b) Tetragonal MnBi with in-plane lattice constants (a and b) matched to GaAs while c is optimized by minimizing the total energy ($a=b=5.65$ Å and $c/a=1.345$); the magnetic moment is $4.000\mu_B$. The deeper valence band from Bi $6s$ is not shown in the figure.

is calculated from the gradient of the potential and the eigenstates are determined by a second variation. That is, a subset of eigenstates calculated without spin-orbit coupling is taken as basis states and a second diagonalization is performed. As pointed out by Kuneš *et al.*,[38] it is important to include local orbitals with $p_{1/2}$ character in the basis since states with the proper form near the nucleus are not obtained in the usual scalar relativistic approximation. Our results for the band structure at Γ are shown in Fig. 7. The symmetry labels are from Parmenter[39] and correspond to the point group T_d. We also include labels from Dresselhaus[40] and Tinkham.[41] We note that in T_d both (x, y, z) and (xy, yz, zx) form basis functions for Γ_{15} (T_2, Γ_4). Basis functions for Γ_{25} (T_1, Γ_5) have f and g character.

We see from Fig. 7 that the top of the valence band is split

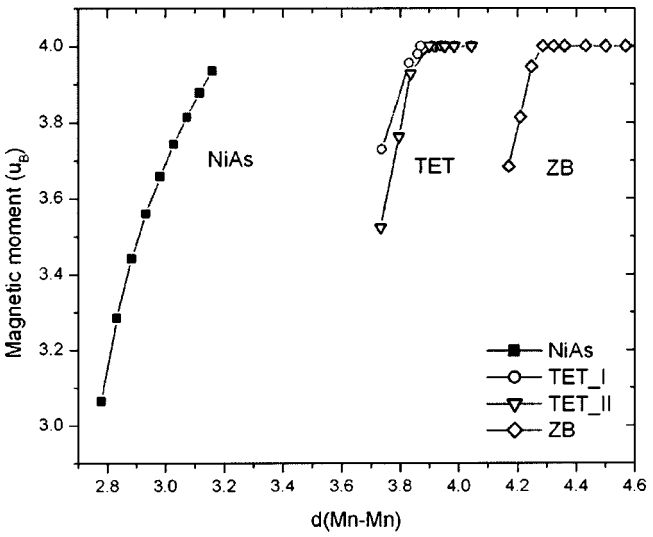

FIG. 6. Magnetic moment of MnSb as a function of Mn-Mn distance, i.e., d(Mn-Mn). In tetragonal structure (TET_I and TET_II), d(Mn-Mn) is the average of lateral and perpendicular bond lengths of Mn-Mn.

into three components as predicted. However, the magnitude of the splitting is only 0.8 eV, even less than ζ. This is due to hybridization. The valence band maximum is a mixture of Bi $6p$ and Mn $3d$ states, which reduces the effective spin-orbit parameter accordingly.

The total energy and moments of the various structures in the presence of spin-orbit coupling are also given in the tables. As noted earlier, the results are not qualitatively affected, although the energy difference between the NA and ZB structures is significantly reduced, which could facilitate the epitaxial growth of the ZB structure.

Finally, we note that as a result of the spin-orbit interac-

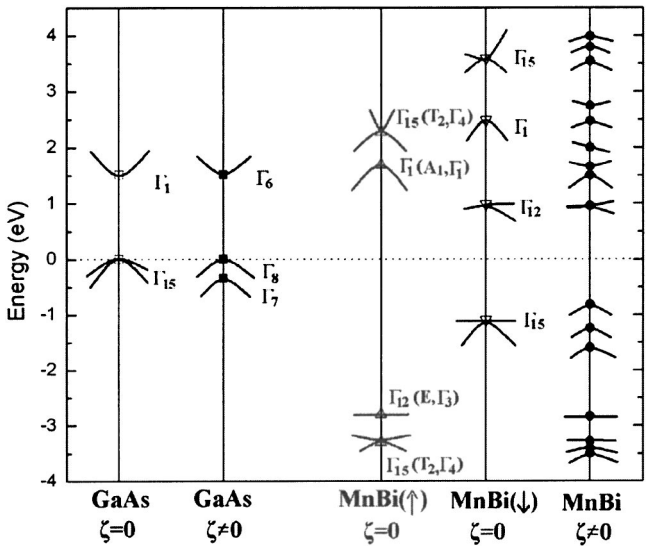

FIG. 7. Effect of exchange and spin-orbit splitting on the band structure of MnBi near Γ. For comparison we also show the bands (experimental band gap is used) for GaAs. The symmetry labels are from Refs. 39–41 as explained in the text; ζ is the spin-orbit coupling parameter.

tion it is not possible to characterize the bands as purely spin up or spin down. An electron injected at the Fermi level with spin up would acquire, on propagation, a spin-down component. Conversely, an electron injected at E_f with spin down could still propagate through the material because it would acquire a spin-up component. This is a fundamental limitation for device design which cannot be totally avoided because there is always some spin-orbit interaction. There would still be a large difference in the conductivity between spin-up and spin-down injection, but the conductivity for spin down would not be precisely zero (of course, thermal, impurity, and disorder effects would also contribute to such ''leakage'').

VI. CONCLUSION

In summary, we have used both full potential and pseudopotential first principles methods to investigate the electronic and magnetic properties as well as the stabilities of MnSb and MnBi in NiAs, ZB, and tetragonal structures. Particular emphasis was focused on the effect of tetragonal distortions (strains) on the magnetic properties. Our calculations lead to some interesting findings: (i) the zinc-blende structure of MnSb and MnBi is mechanically unstable, and would transform spontaneously into a metastable denser tetragonal phase with c/a less than 1 or larger than 1; (ii) the tetragonal phase with $c/a<1$ is more stable than that with $c/a>1$, and its density is comparable with that of the hexagonal NiAs phase; (iii) MnSb and MnBi compounds in the ZB structure and tetragonal phases are both half-metallic ferromagnets; (iv) the spin-orbit splitting is less than might have been expected because of magnetic effects. We also find that the property of half-metallic ferromagnetism is maintained over a larger volume range for the tetragonal structures than for the cubic structure, suggesting that it may be possible to grow such films epitaxially on semiconductor substrates with a wide range of lattice constants, including GaAs.

ACKNOWLEDGMENTS

The authors are very grateful for fruitful discussions with Dr. N. Stojic. The work at Brookhaven was supported by U.S. Department of Energy under Contract No. DE-AC02-98CH10886.

[1] T. Dietl, H. Ohno, F. Matsukura, J. Cibert, and D. Ferrand, Science **287**, 1019 (2000).
[2] S. A. Wolf, D. D. Awschalom, R. A. Buhrman, J. M. Daughton, S. von Molnár, M. L. Roukes, A. Y. Chtchelkanova, and D. M. Treger, Science **294**, 1488 (2001).
[3] S. Datta and B. Das, Appl. Phys. Lett. **56**, 665 (1990).
[4] G. Prinz, Science **282**, 1660 (1998).
[5] G. Burkard, D. Loss, and D. P. DiVincenzo, Phys. Rev. B **59**, 2070 (1999).
[6] Y. Q. Xu, B. G. Liu, and D. G. Pettifor, Phys. Rev. B **66**, 184435 (2002).
[7] J. W. Dong, L. C. Chen, C. J. Palmstrom, R. D. James, and S. McKernan, Appl. Phys. Lett. **75**, 1443 (1999).
[8] S. M. Watts, S. Wirth, S. von Molnár, A. Barry, and J. M. D. Coey, Phys. Rev. B **61**, 9621 (2000).
[9] F. J. Jedema, A. T. Filip, and B. van Wees, Nature (London) **410**, 345 (2001); S. Soeya, J. Hayakawa, H. Takahashi, K. Ito, C. Yamamoto, A. Kida, H. Asano, and M. Matsui, Appl. Phys. Lett. **80**, 823 (2002).
[10] J. M. D. Coey, M. Viret, and S. von Molnár, Adv. Phys. **48**, 169 (1999).
[11] S. Sanvito and N. A. Hill, Phys. Rev. B **62**, 15 553 (2000).
[12] A. Continenza, S. Picozzi, W. T. Geng, and A. J. Freeman, Phys. Rev. B **64**, 085204 (2001).
[13] Y. J. Zhao, W. T. Geng, and A. J. Freeman, Phys. Rev. B **65**, 113202 (2002).
[14] W. H. Xie, Y. Q. Xu, B. G. Liu, and D. G. Pettifor, Phys. Rev. Lett. **91**, 037204 (2003).
[15] W. H. Xie, B. G. Liu, and D. G. Pettifor, Phys. Rev. B **68**, 134407 (2003).
[16] A. Janotti, S. H. Wei, and L. Bellaiche, Appl. Phys. Lett. **82**, 766 (2003).
[17] I. Galanakis and P. Mavropoulos, Phys. Rev. B **67**, 104417 (2003).
[18] J. E. Pask, L. H. Yang, C. Y. Fong, W. E. Pickett, and S. Dag, Phys. Rev. B **67**, 224420 (2003).
[19] A. Debernardi, M. Peressi, and A. Baldereschi, Comput. Mater. Sci. **27**, 175 (2003).
[20] B.-G. Liu, Phys. Rev. B **67**, 172411 (2003).
[21] P. Hohenberg and W. Kohn, Phys. Rev. **136**, B864 (1964); W. Kohn and L. J. Sham, Phys. Rev. **140**, A1133 (1965); R. G. Parr and W. T. Yang, *Density-Functional Theory of Atoms and Molecules* (Oxford University Press, New York, 1989).
[22] P. Blaha, K. Schwarz, G. Madsen, D. Kvasnicka, and J. Luitz, Computer code WIEN2K, Technische Universitat Wien, Austria, 2001.
[23] J. P. Perdew, K. Burke, and M. Ernzerhof, Phys. Rev. Lett. **77**, 3865 (1996).
[24] P. Ordejón, E. Artacho, and J. M. Soler, Phys. Rev. B **53**, 10 441 (1996).
[25] J. M. Soler, E. Artacho, J. D. Gale, A. García, J. Junquera, P. Ordejón, and D. Sánchez-Portal, J. Phys.: Condens. Matter **14**, 2745 (2002).
[26] N. Troullier and J. L. Martins, Phys. Rev. B **43**, 1993 (1991).
[27] L. Kleinman and D. M. Bylander, Phys. Rev. Lett. **48**, 1425 (1982).
[28] S. G. Louie, S. Froyen, and M. L. Cohen, Phys. Rev. B **26**, 1738 (1982).
[29] H. J. Monkhorst and J. D. Pack, Phys. Rev. B **13**, 5188 (1976).
[30] R. A. de Groot, F. M. Mueller, P. G. van Engen, and K. H. J. Buschow, Phys. Rev. Lett. **50**, 2024 (1983).
[31] J.-C. Zheng, M. C. Payne, Y. P. Feng, and A. T.-L. Lim, Phys. Rev. B **67**, 153105 (2003).
[32] (a) *Numerical Data and Functional Relationships in Science and Technology*, edited by K. Adachi and S. Ogawa, Landolt-Börnstein, New Series, Group III, Vol. 27, pt. a (Spinger-Verlag, Berlin, 1988); (b) J. B. Yang, K. Kamaraju, W. B. Yelon, W. J.

James, Q. Cai and A. Bollero, Appl. Phys. Lett. **79**, 1846 (2001).
[33] K. Ono, J. Okabayashi, M. Mizuguchi, M. Oshima, A. Fujimori, and H. Akinaga, J. Appl. Phys. **91**, 8088 (2002).
[34] H. Akinaga, T. Manago, and M. Shirai, Jpn. J. Appl. Phys., Part 2 **39**, L1118 (2000).
[35] M. Mizuguchi, H. Akinaga, T. Manago, K. Ono, M. Oshima, M. Shirai, M. Yuri, H. J. Lin, H. H. Hsieh, and C. T. Chen, J. Appl. Phys. **91**, 7917 (2002).
[36] J. H. Zhao, F. Matsukura, K. Takamura, E. Abe, D. Chiba, and H. Ohno, Appl. Phys. Lett. **79**, 2776 (2001).
[37] M. L. Cohen and J. R. Chelikowsky, *Electronic Structure and Optical Properties of Semiconductors* (Springer-Verlag, Berlin, 1989), pp. 45 and 49.
[38] J. Kuneš, P. Novák, R. Schmid, P. Blaha, and K. Schwarz, Phys. Rev. B **64**, 153102 (2001).
[39] R. H. Parmenter, Phys. Rev. **100**, 573 (1955).
[40] G. Dresselhaus, Phys. Rev. **100**, 580 (1955).
[41] M. Tinkham, *Group Theory and Quantum Mechanics* (McGraw-Hill, New York, 1964).
[42] *Numerical Data and Functional Relationships in Science and Technology*, edited by O. Madelung, Landolt-Börnstein, New Series, Group III, Vol. 22, pt. a (Springer-Verlag, Berlin, 1987).